Microporous and Mesoporous Materials 349 (2023) 112422

Contents lists available at ScienceDirect

Microporous and Mesoporous Materials

journal homepage: www.elsevier.com/locate/micromeso

Degradation of pollutants in water by Fenton-like oxidation over LaFe-catalysts: Optimization by experimental design

Ouissal Assila [a,b], Óscar Barros [a,c,d], António M.F. Fonseca [a,c,d], Pier Parpot [a,c,d], Olívia S.G. P. Soares [e,f], Manuel F.R. Pereira [e,f], Farid Zerrouq [b], Abdelhak Kherbeche [b], Elizabetta Rombi [g], Teresa Tavares [c,d], Isabel C. Neves [a,c,d,*]

[a] CQUM, Centre of Chemistry, Chemistry Department, University of Minho, Campus de Gualtar, 4710-057, Braga, Portugal
[b] Laboratory of Catalysis, Process, Materials and Environment, School of Technology, University Sidi Mohammed Ben Abdellah Fez, Morocco
[c] CEB - Centre of Biological Engineering, University of Minho, Campus de Gualtar, 4710-057, Braga, Portugal
[d] LABBELS – Associate Laboratory, Braga, Guimarães, Portugal
[e] LSRE-LCM - Laboratory of Separation and Reaction Engineering – Laboratory of Catalysis and Materials, Faculty of Engineering, University of Porto, Portugal
[f] ALiCE - Associate Laboratory in Chemical Engineering, Faculty of Engineering, University of Porto, Portugal
[g] Dipartimento di Scienze Chimiche e Geologiche, University of Cagliari, Complesso Universitario di Monserrato, 09042, Monserrato, Italy

ARTICLE INFO

Keywords:
Box-Behnken design
La^{3+}/Fe^{3+}
Heterogeneous catalysts
Pollutants
Fenton-like oxidation
Mineralization

ABSTRACT

The effect of different parameters such as temperature, type of catalyst and hydrogen peroxide (H_2O_2) concentration on the degradation of pollutants in water by Fenton-like oxidation was studied by using the Box-Behnken design (BBD), an effective statistical model to design the experiments. Concerning the heterogeneous catalysts, three bimetallic catalysts with lanthanum (La) and iron (Fe) ion-exchanged into zeolites (NaY and ZSM5) and a natural clay from Morocco were prepared and used for Fenton-like oxidation of organic pollutants in water. Tartrazine (Tar, a food coloring compound known as E102) and caffeine (Caf, a stimulant drug present in popular beverages such as coffee and tea) were selected as pollutants due to their presence in several commercial products for daily consumption. The BBD model indicated that the optimum catalytic conditions for Fenton-like reaction with an initial pollutant concentration of 30 ppm at pH 3.0 were T = 40 °C and 90 mM of H_2O_2. The maximum conversion values achieved with the best catalyst, LaFeZSM5, were 96.6% for Tar after 180 min and 51.0% for Caf after 300 min of reaction. To increase the conversion of Caf, a modified zeolite electrode was used for electro Fenton-like oxidation without H_2O_2, at room temperature.

1. Introduction

Doping of inorganic materials with rare-earth ions can improve different properties, making the resulting new materials very attractive for technological applications, especially in the field of catalysis [1]. The rare-earth elements (REE) are a group of seventeen elements (lanthanides group of the periodic table with scandium and yttrium in addition). Lanthanum (La) is abundant in natural storage and could be used as a more cost-effective catalyst than the other sixteen REE. Lanthanide-doped nanoparticles have attracted extensive attention for their unique properties and prospective applications in optical materials, photocatalysis and photonic band gap materials [1,2]. Lanthanum oxide, which can contribute with both base and acid properties to the binary catalyst system, is customarily used as a catalyst, co-catalyst or catalyst promoter [3–5]. La^{3+} is recognized to enhance the photocatalytic activity of $LaFeO_3$ nanoparticles towards photodegradation of dye compounds under visible light irradiation, due to the synergistic effect between the semiconductor photocatalysis and the Fenton-like reaction [6]. Also, the presence of La^{3+} ions in La–Na–Cu–O perovskite-like complex oxide catalysts prepared by the sol-gel auto--combustion method enhances the removal of soot and simultaneously accelerates NO_x reactions [7]. Recently, La-doped carbon nitride single-atom catalysts with a La–N charge-transfer bridge were prepared and evaluated in the photocatalytic reduction of CO_2 to CO, which in turn can be converted into solar fuels. The resulting catalysts exhibited high CO yielding rate, with good selectivity and stability compared to most reported carbon nitride-based photocatalysts [8].

Several studies with REE-containing zeolites were performed in

* Corresponding author. CQUM, Centre of Chemistry, Chemistry Department, University of Minho, Campus de Gualtar, 4710-057, Braga, Portugal.
E-mail address: ineves@quimica.uminho.pt (I.C. Neves).

https://doi.org/10.1016/j.micromeso.2022.112422
Received 2 November 2022; Received in revised form 20 December 2022; Accepted 23 December 2022
Available online 28 December 2022

recent years to assess the selectivity and stability of the catalysts [9]. The presence of REE in the Y zeolite reduces the framework dealumination under hydrothermal conditions, increasing the zeolite activity and enhancing the hydrogen transfer rate. One example of such is the conversion of hydrocarbon fractions of crude petroleum oils to more valuable products [10,11]. In addition, the ternary $CuCeFeO_x$ catalysts supported on zeolite/PSF displayed a good conversion in the oxidation of CO to CO_2, following a pseudo-first-order kinetic law [12].

In the advanced oxidation processes for wastewater treatment, photocatalysis, ozonization, and Fenton oxidation using metal-support as heterogeneous catalysts have been applied successfully for the removal or degradation of recalcitrant pollutants [13–17]. Fenton reaction is characterized by the presence of ferrous salt and hydrogen peroxide to form radical hidroxyls ($OH^{\bullet}$) wich turn in the rapid degradation of pollutants [15–17].

The use of heterogeneous Fenton-like catalysts has had great attention due to their low cost, eco-compatibility, operational mild conditions (20-50 °C, wide pH range and atmospheric pressure), and high efficiency [15–19]. These heterogeneous catalysts offer a great stability of the active centres, present limited leaching of metals from the catalyst, are easy recoverable from the reaction medium, and can be regenerated by a suitable activation procedure [15–17]. In addition, the utilization of clays or zeolites as catalysts for Fenton-like reaction is very attractive, due to the selective sorption capacities, non-toxic nature, availability, and low cost [15–17,19,20] of these porous materials.

La–Fe montmorillonite was prepared by a precipitation method to work as a heterogeneous catalyst on the degradation of rhodamine B (RhB) and methylene blue (MB) dyes, using Fenton-like oxidation in both batch and fixed-bed set-ups. The catalyst exhibited high dyes conversions, with 96% and 97% degradation of the RhB and MB initially present (100 mg/L), respectively [19]. In the case of zeolites, Cu(II) or Mn(II) were ion-exchanged together with Fe(III) ions in NaY zeolite and used as bimetallic catalysts in Fenton-like oxidation for removing two dye compounds (procion yellow (PY) and tartrazine (Tar)). CuFe–NaY and MnFe–NaY displayed the best mineralization rates for PY and for Tar degradation [20].

The goal of this work is to select the best heterogeneous catalyst based in two zeolite structures, MFI and FAU, and a natural clay from Morocco, with La and Fe for the degradation of tartrazine (Tar) and caffeine (Caf) pollutants in water by Fenton-like oxidation. For this study, the experimental reaction conditions were optimized using a statistical model. The Response Surface Methodology (RSM) is a statistical approach to analyze and reduce the number of experiments to give the optima of independent parameters in the reaction [21,22]. Central composite, Doehlert and Box-Behnken design (BBD) are three classes of response surface designs. Box-Behnken design is more advantageous than the others since it makes the experiments economically feasible and beneficial for optimization of different organic matter treatment processes [23].

Bearing this in mind, the work was performed in four phases: (i) preparation of the heterogeneous catalysts by ion-exchanging La(III) and Fe(III) into the solid supports; (ii) optimization of the experimental conditions for Fenton-like oxidation using the BBD model; (iii) evaluation of the stability and reusability of the best catalyst for both pollutants, and (iv) performance of electro Fenton-like oxidation using the best catalyst as a modified electrode to enhance the degradation of the Caf pollutant. The best catalyst selected from BBD model was LaFeZSM5, which presents high degradation of Tar by a typical Fenton-like oxidation. Finally, the degradation of Caf was enhanced using the electro Fenton-like oxidation at room temperature without hydrogen peroxide (H_2O_2).

2. Experimental

2.1. Materials and chemicals

(NH_4)ZSM5 (CBV3024E, Si/Al = 15.00), NaY (CBV100, Si/Al = 2.83) zeolites were obtained from Zeolyst International in powdered form. A natural Moroccan clay was achieved from the Middle Atlas region ($Clay_M$, where M stands for Morocco). It was dried at 100 °C overnight and then crushed up to 63 μm, prior to use. The compounds: tartrazine (Tar, $C_{16}H_9N_4Na_3O_9S_2 \geq 90\%$), caffeine (Caf, $C_8H_{10}N_4O_2 \geq 99\%$), sodium bisulphite ($Na_2SO_3$), hydrochloric acid (HCl, ≥99.5%), sodium hydroxide (NaOH, ≥99.0%) and absolute ethanol (C_2H_5OH, ≥99.7%) were provided by Sigma Aldrich. Lanthanum (III) nitrate ($La(NO_3)_3 6H_2O$, 99.9%, Alfa Aesar), iron (III) nitrate ($Fe(NO_3)_3 9H_2O$, Aldrich), hydrogen peroxide (H_2O_2, 30 wt%, Merck), phosphoric acid (H_3PO_4, analytical reagent, ≥85%), and oxalic acid ($C_2H_2O_4$, ≥99.5%) were used as received. Deionized water was produced with an ultrapure water system (Milli-Q, EQ 7000).

2.2. Catalyst preparation

The catalysts were prepared by an ion-exchange method using the adapted procedure described elsewhere [24,25]. Aqueous solutions (250 mL) containing different lanthanum amounts (0.90×10^{-2} mmol for (NH_4)ZSM5 and $Clay_M$, and 2.70×10^{-2} mmol for NaY) were mixed with 4 g of the pristine support at pH 4. The suspensions were stirred during 24 h at room temperature. 1.5 g of the La-containing zeolite samples, LaNaY and LaZSM5, were added to 250 mL of iron solution (4.48×10^{-2} mmol) and then submitted to the same procedure as before to obtain the bimetallic LaFeNaY and LaFeZSM5 samples. In the case of the Moroccan clay as the support, due to the initial presence of iron in its structure, the bimetallic $LaFeClay_M$ sample was obtained by ion exchange only with lanthanum. After each ion-exchange step, the suspensions were filtered-off, washed with deionized water and dried in an oven at 60 °C overnight. Finally, the solids were calcined in an oven at 350 °C during 4 h under a dry-air stream.

2.3. Characterization

The textural characterization of the catalysts was performed by N_2 adsorption isotherms, determined at −196 °C with a Nova 4200e (Quantachrome Instruments) equipment. The samples were degassed at 150 °C during 3 h. The micropore volumes (V_{micro}) and mesopore surface areas (S_{meso}) were calculated by the t-method. Surface areas were calculated with the BET equation.

The morphology of the samples was characterized using a scanning electron microscope (SEM, FORMAT JEOL/EO) coupled with energy-dispersive X-ray spectroscopy (EDX). In order to avoid surface charging, samples were coated with gold in vacuum prior to analysis, by using a Fisons Instruments SC502 sputter coater.

Elemental analysis was performed by inductively coupled plasma atomic emission spectroscopy (ICP-AES) for the quantification of lanthanum in the liquid phase during the ion-exchange method by ICP-OES spectrometer (Optima 8000, PerkinElmer). The same analysis was performed to quantify the La, Fe, Si, Al and Na in the solid samples with a 5110 ICP-OES spectrometer (Agilent Technologies). Solid samples (ca. 0.05 g) were thermally treated at 500 °C for 12 h to remove the adsorbed water and subsequently placed in a platinum crucible. Then, the melting agent was added ($Li_2B_4O_7$:sample = 15:1 by weight), and the alkaline fusion was carried out in a muffle furnace at 1000 °C for 40 min. After cooling of the melt, the resultant fusion bead was transferred into a beaker and heated on a plate at 80 °C after addition of 100 mL of 5% HNO_3 (all the samples were found to completely dissolve within 40 min). Finally, the solution was transferred into a volumetric flask (250 mL) and diluted to the desired final volume with milliQ water.

Fourier Transform Infrared, FTIR, spectroscopy measurements of the

samples were carried out using a PerkinElmer Spectrum Two spectrometer, equipped with an ATR accessory. A diamond prism was used as the waveguide. All spectra were recorded with a resolution of 4 cm^{-1} in the wavelength region 4000-400 cm^{-1} by averaging 16 scans and the analyses were carried out at room temperature.

Temperature programmed reduction (TPR) experiments were carried out in an AMI-200 (Altamira Instruments) apparatus. The sample (about 100 mg) was placed in a U-shaped quartz tube located inside an electrical furnace and heated at 5 °C min^{-1} up to 600 °C under a flow of 5% (v/v) H_2 diluted with He (total flow rate of 30 cm^3 (STP) min^{-1}). The H_2 consumption was followed by a thermal conductivity detector (TCD).

2.4. Experimental design

To optimize the experimental conditions for the degradation of the organic pollutants by the Fenton-like reaction, a statistical approach was applied using the Box-Behnken Design (BBD) model. This design expert software allowed the set of batch experiments to be developed. Three factors of three levels - (i) catalysts (X_1: LaFeNaY, $LaFeClay_M$ and LaFeZSM5), (ii) temperature (X_2: 30 °C, 40 °C and 50 °C) and (iii) concentration of hydrogen peroxide (X_3: 45, 90 and 135 mM) - were used to determine the model coefficients in quadratic terms (Table 1). The predicted response, Y_m, represents the variables Tar (Y_1) and Caf (Y_2) calculated by equation (1):

$$Y_m = \beta_0 + \sum_{i=1}^{k} \beta_i X_i + \sum_{i=1}^{k-1} \sum_{j=2}^{k} \beta_{ij} X_i X_j + \sum_{i=1}^{k} \beta_{ii} X_i^2 + \varepsilon \quad \text{(Eq. 1)}$$

where β_0 is the intercept coefficient; β_i, β_{ii}, and β_{ij} (with i = 1, 2, 3; j = 1, 2, 3) are the linear coefficients, squared coefficients and interaction coefficients, respectively. X_i and X_j are the coded independent variables and ε is the random error [21,23].

2.5. Catalytic tests

Catalytic tests were carried out in a semi-batch reactor at atmospheric pressure under stirring. Prior to experiments, the catalysts were pretreated at 100 °C for 2 h in an oven. The semi-batch reactor was loaded with 250 mL of a 30 ppm solution of Tar or Caf, at pH = 3, using 200 mg of catalyst and 5 mL of H_2O_2 at a specific concentration and temperature (Table 1). The reaction was then performed under stirring at 300 rpm, during 180 and 300 min for Tar and Caf, respectively, due to be the best reaction time for the degradation. Sampling was carried out at fixed time intervals and the reaction was stopped with the addition of an excess of $NaHSO_3$, which instantaneously consumes the unreacted H_2O_2. Catalytic tests were performed in duplicate, and the maximum deviation observed in the removal of the organic pollutants was 2%.

The stability of the best catalyst for Tar and Caf degradation was studied using the experimental catalytic conditions determined above. Four cycles were performed and after each cycle the catalyst was filtered-off, washed with ethanol and dried in an oven at 70 °C overnight before reutilization. FTIR and SEM analyses were carried out in order to verify the stability of the support structure, while the possible leaching of metals after the cycle reactions was checked by EDX analyses. The amounts of La and Fe eventually leached during the reaction were also measured by ICP-OES spectrometer (Optima 8000, PerkinElmer).

Table 1
Independent factors and levels used for Box-Behnken design for Tar and Caf degradation.

Coded factor	Factor	Coded level		
		−1	0	+1
X_1	Type of catalyst	LaFeNaY (1)	$LaFeClay_M$ (2)	LaFeZSM5 (3)
X_2	T (°C)	30	40	50
X_3	$[H_2O_2]$ (mM)	45	90	135

After centrifugation, the solution was analyzed in order to quantify the degradation of the organic pollutants with the help of UV–vis and TOC analyses. An UV–vis spectrophotometer (UV–2501PC from Shimadzu) was used at the characteristic wavelengths λ_{max} = 427 nm and 272 nm for Tar and Caf, respectively [20,26,27].

The total organic carbon (TOC) was determined using the NPOC method, with a Shimadzu's Total Organic Carbon Analyzer TOC-L, coupled with the ASI-L autosampler of the same brand.

2.6. Electrochemistry

The best bimetallic catalyst was used as a modified electrode for the electro-Fenton-like degradation of Caf at room temperature. The modified electrode was prepared by the addition of 20 mg of the bimetallic catalyst to a mixture of ultra-pure water (Millipore system, 18.2 MΩ cm at 20 °C) and Nafion® suspension (5 wt % Sigma-Aldrich®). The resulting catalytic ink was homogeneously deposited onto the wet proofed Toray carbon paper with an area of 2 cm × 2 cm. Finally, the carbon Toray paper was glued to the platinum electrode using conductive carbon cement (Quintech) and was dried at room temperature for 24 h.

Electrochemical measurements were performed as described elsewhere [24,28,29]. The electroactivity of the modified electrode was investigated by cyclic voltammetry (CV) in the absence and in the presence of Caf in Na_2SO_4 (0.10 M). Electro Fenton-like oxidation at a constant potential of 2.0 V *vs.* SCE, in the presence of Caf (100 ppm), was carried out in a two-compartment cell separated with an ion exchange membrane (Nafion®-417, membrane thickness 0.017 inches) that separates the anode and cathode compartments.

A high performance liquid chromatograph (HPLC), equipped with an isocratic pump (Jasco PU-980 Intelligent HPLC Pump) and a double online detection including an UV–vis detector (Jasco Intelligent), was used for quantifying Caf at 272 nm, i.e. at the maximum of Caf absorption reported in the literature [21,30,31]. An ion exchange column (Aminex HPX-87H by Biorad) and a mobile phase consisting of 1.8 × 10^{-3} M sulfuric acid with a flow of 0.8 mL/min were used for the separation of reaction products.

Electrolysis products from Caf degradation were identified using a HPLC-MS system (Thermo LxQ) with a C-18 (150 × 4.6 mm) column. The low molecular weight organic acids were identified by HPLC analysis using the same equipement described before.

3. Results and discussion

3.1. Statistical analysis and optimal conditions for pollutants degradation

In order to elucidate the importance of the different parameters and to determine the optimal experimental conditions for efficient oxidation by Fenton-like reaction, the Box-Behnken design (BBD) model was used.

The experimental design for calculating the percentage of the pollutants conversion (Y, Eq. (1)), as the response of the design experiments with three variables - type of the catalyst, temperature and concentration of hydrogen peroxide - chosen for optimization the degradation of pollutants by Fenton-like reaction (Table 1) were performed with three central replicates. Table 2 provides the matrix for predicting the number of experimental runs to obtain responses in terms of tartrazine (Tar) and caffeine (Caf) conversions, with the number of the optimized factors k equal three variables and C_0 is the central value using equation (2), where a total of 15 experiments were performed [32,33]. The results corresponde to the combined effect of three factors in their specified range.

$$N = 2 \times k \times (k-1) + C_0 \quad \text{(Eq. 2)}$$

The analysis of variance (ANOVA) findings was carried out to evaluate the validity of the statistical model testing (Table S1). In ANOVA, the most parameters tested to assess the model validation are the ratio

Table 2
Box-Behnken design for the three independent variables with the conversion (%) of the compounds.

Experiments	catalyst	T (°C)	[H_2O_2] (mM)	X_{Tar} (%)	X_{Caf} (%)
1	1	30	90	17.47	21.57
2	3	30	90	62.98	36.15
3	1	50	90	27.08	32.06
4	3	50	90	96.58	51.03
5	1	40	45	20.01	25.29
6	3	40	45	85.46	41.16
7	1	40	135	33.51	30.22
8	3	40	135	96.82	45.12
9	2	30	45	31.21	30.93
10	2	50	45	40.66	43.04
11	2	30	135	45.75	29.15
12	2	50	135	65.60	42.27
13	2	40	90	53.83	34.97
14	2	40	90	54.40	35.34
15	2	40	90	53.37	35.50

values of model's mean-square, the F-values signified and the confidence interval P-values of model terms were computed at 95%, which means that P- value < 5% insured the model's significance. Hence, the higher F-values (67.67% for Tar and 27.05% for Caf conversion), in addition to the low p-values (<0.001) for both the pollutants, confirm that the statistical validation was of high significance. Moreover, the values of correlation coefficients (R^2) were very high (Tar: $R^2 = 0.9919$ with Adj $R^2 = 0.9772$ and Caf: $R^2 = 0.9799$ and Adj $R^2 = 0.9436$, Table S1), demonstrating that the application of the developed model is well fitted to the experimental values and highly predictive [34]. Furthermore, the results illustrated in Fig. 1a (Tar) and 1b (Caf) revealed high correlation between the predicted and the experimental values of Tar and Caf conversions, respectively, indicating that the model is suitable and has a good performance for the response of both pollutants degradation.

Accordingly, the second order polynomial relation that allowed also the determination of the regression between the three different factors and the response Tar (Y_1) and Caf (Y_2) conversion was expressed by equations (3) and (4):

$$Y_1 = 53.88 + 30.47X_1 + 9.06X_2 + 8.04X_3 + 6 \times 1 \times 2 - 0.5361 \times 1 \times 3 + 2.6 \times 2 \times 3 + 5.15 \times 1^2 - 8 \times 2^2 - 0.0728 \times 3^2 \quad \text{(Eq. 3)}$$

In the Tar degradation, the most important factor is the catalyst type, and the interaction between catalyst type and H_2O_2 concentration is not important in this case.

$$Y_2 = 35.27 + 8.04X_1 + 6.33X_2 + 0.7925X_3 + 1.1 \times 1 \times 2 - 0.2425 \times 1 \times 3 + 0.2525 \times 2 \times 3 - 0.4838 \times 1^2 + 0.4163 \times 2^2 + 0.6612 \times 3^2 \quad \text{(Eq. 4)}$$

For Caf degradation, it seems that the H_2O_2 concentration is not important compared to other factors.

Three dimensional (3D) response surface plots (RSP) for Tar and Caf degradation *versus* type of LaFe-catalyst, temperature and concentration of hydrogen peroxide are shown in Fig. 2.

The best performances of Tar and Caf degradation by Fenton-like reaction were achieved at 40 °C (Fig. 2C and F) at pH = 3, which is considered satisfactory for a reaction temperature in order to achieve the best compromise for a better degradation [20,35,36]. Fig. 2B (Tar) and 2E (Caf) show the effect of the initial concentration of H_2O_2 on the pollutants degradation and, when changing the concentration from 45 to 135 mM, the differences observed had similar influence on the reaction rate. Among the three catalysts used, LaFeNaY, $LaFeClay_M$ and LaFeZSM5, RSP indicate that the conversion rate reaches the best results with the catalyst LaFeZSM5, after 180 min and 300 min for Tar and Caf, respectively (Fig. 2A (Tar) and 2D (Caf)). Remarkably, the performance of the catalysts for both pollutants decreases in the order: LaFeZSM5 > $LaFeClay_M$ > LaFeNaY.

Table 3 shows the optimal conditions determined by using the Box-Behnken design for obtaining the maximum pollutants' degradation by Fenton-like oxidation.

The most efficient catalyst was LaFeZSM5 with a predicted degradation of up to 96.6% of Tar and 51.0% of Caf, after 180 min and 300 min, respectively, under the following experimental conditions: initial concentration of pollutant, 30 ppm, pH 3, H_2O_2 concentration, 90 mM and T = 40 °C. These results demonstrate that the response surface methodology can be helpful as a tool to optimize the experimental conditions for the degradation of pollutants mediated by Fenton-like process.

The introduction of the metal ions by ion-exchange method does not seem to affect the morphology of the supports, as shown by scanning electron microscopy (SEM) images (Fig. 3).

The heterogeneous catalysts present the same morphology of the pristine supports and keep the same average particle size, indicating that the ion-exchange method is appropriate. The presence of La and Fe species in the LaFe-bimetallic catalysts was also investigated by energy-dispersive X-ray (EDX) analysis, which confirms the presence of these metal species in the LaFe-bimetallic catalysts (Fig. S1).

The amount of La still present in the solution after the ion-exchange process was quantified by ICP-AES in order to evaluate the amount of metal loaded by the difference between the initial and the final concentration. The results show that only 15% and 30% of the initial concentration of La was ion-exchanged in ZSM5 and in $Clay_M$, respectively, while 99% of La was ion-exchanged in NaY. The difference in La loading between the two zeolite-based samples is mainly due to the higher Si/Al ratio of ZSM5 compared to NaY, which results in a lower ion exchange capacity of the former zeolite. ICP-AES analyses performed on the solid

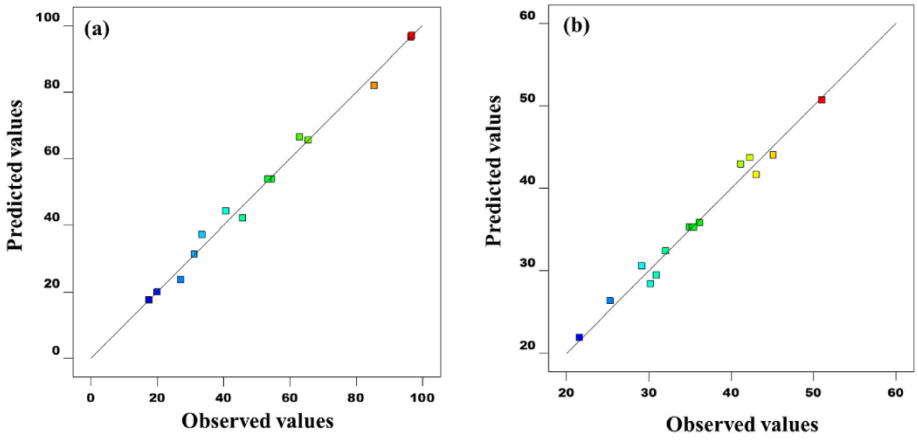

Fig. 1. Predicted values versus actual model values for (a) Tar and (b) Caf.

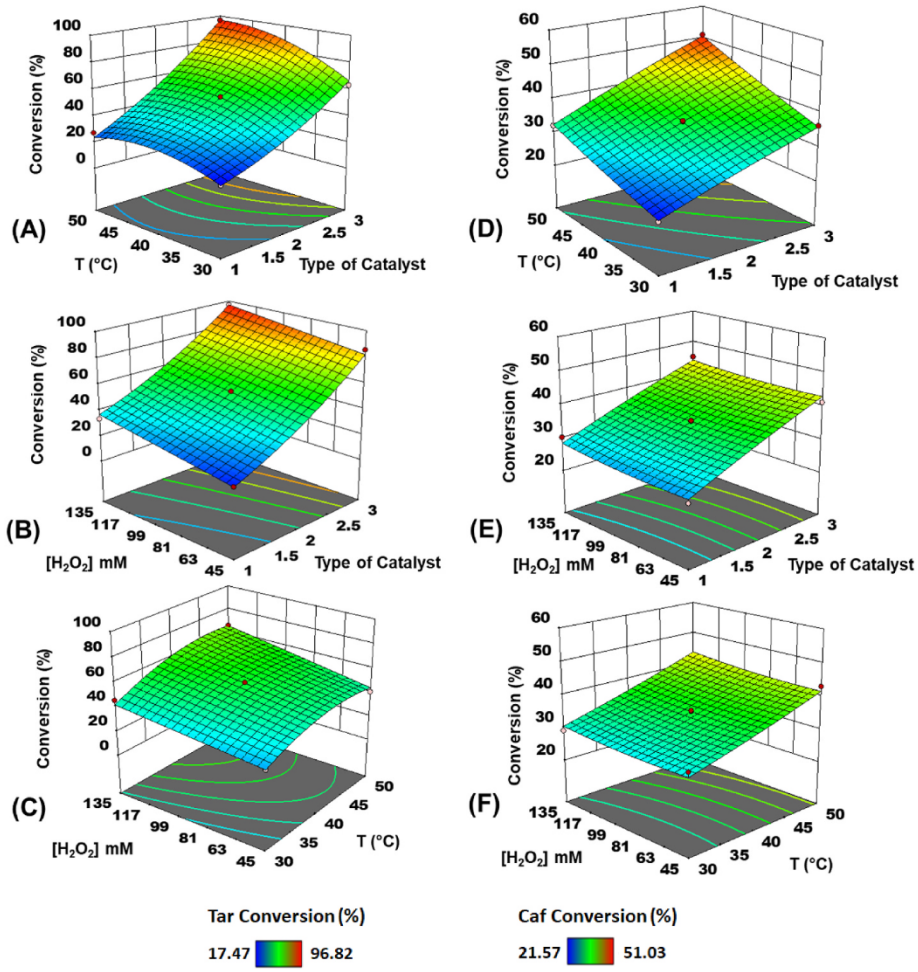

Fig. 2. Response Surface Plots: Effect of the three parameters studied (A, B, C for Tar conversion) and (D, E, F for Caf conversion).

Table 3
Predicted and experimental values of Tar and Caf conversion under optimal conditions.

Coded factor	Factor	Value	Optimum combination of the model (X, %)		Experimental validation of the model (X, %)	
X_1	catalyst	LaFeZSM5	X_{Tar}	X_{Caf}	X_{Tar}	X_{Caf}
X_2	T (°C)	40	96.56	50.66	96.60	51.00
X_3	$[H_2O_2]$ (mM)	90				

X = conversion in percentage.

catalysts to determine their chemical composition (Tables S2 and S3) confirm the low La content for LaFeZSM5 (0.0011 wt%) with respect to LaFeNaY (0.18 wt%), whereas equal Fe contents are detected (0.26 wt% for LaFeZSM5 and LaFeNaY). Noteworthy, a decrease in the Si/Al ratio can be observed for the ion-exchanged NaY samples, which suggests that the acidic medium affects the FAU structure. In the case of the clay-supported catalyst, a low amount of La is ion-exchanged (0.003 wt%), while the amount of Fe seems to be not affected by the ion exchange procedure, being equal to 5.87 and 5.94 wt% for $LaFeClay_M$ and $Clay_M$, respectively.

The intermediary catalytic behavior of $LaFeClay_M$ determined by the BBD model could be ascribed to the low amount of La and to the presence of iron most probably in the form of iron oxide. It is common sense that the nature of acidic sites in clays is different from those of metal oxides and zeolites [37]. In the binary acid-base CaO–La_2O_3 catalyst, the different La species affect the catalytic properties, where the surface lattice oxygen in the lanthanum oxide is attributed to the Lewis base sites and the metal ions La^{3+} are Lewis acid sites [38]. Clay materials have higher amounts of Lewis than of Brønsted acid sites, so they have a lower acidity than zeolites, despite being higher than NaY. This fact could also be ascribed to the larger amount of iron present in the natural clay, 5.87 wt% for $LaFeClay_M$, as well as to the presence of other metals, Ti (0.46 wt%) and Mg (0.71 wt%).

The lower activity of LaFeNaY could be assigned to the desalumination of the zeolite and to the different acidic behavior of NaY zeolite. Both pristine zeolites present Brønsted and Lewis acid sites characteristic of these structures with a different sites strength distribution: 97% of weak sites, 2% medium sites and only 1% of strong sites were assessed to NaY; in the case of ZSM5, the distribution was 46.5% of weak sites, 48.2% medium sites and 5.3% of strong sites [39]. The higher number of strong and medium-strength acidic sites of ZSM5 (53.5%) enhances its performance compared to NaY (3%) and to the natural clay [40]. The improved efficiency of LaFeZSM5 could be attributed to the fact that the presence of La species together with Fe species contributes to the acid properties in the catalyst system. In addition, the presence of the iron (III) extra framework increases the catalytic activity of the ZSM5 [41] as show by Fourier transform infrared (FTIR) spectroscopy analysis. The typical bands of the pristine supports (Fig. 4) dominate all the FTIR spectra of the prepared catalysts.

In the case of $Clay_M$, the band at 3625 cm^{-1} is assigned to the –OH stretching vibration of the structural hydroxyl groups; the band at 1035 cm^{-1} is due to the in-plane bending vibration of Si–O–Si and the bands at 920, 885, 850 and 520 cm^{-1} are attributed to the stretching vibrations of

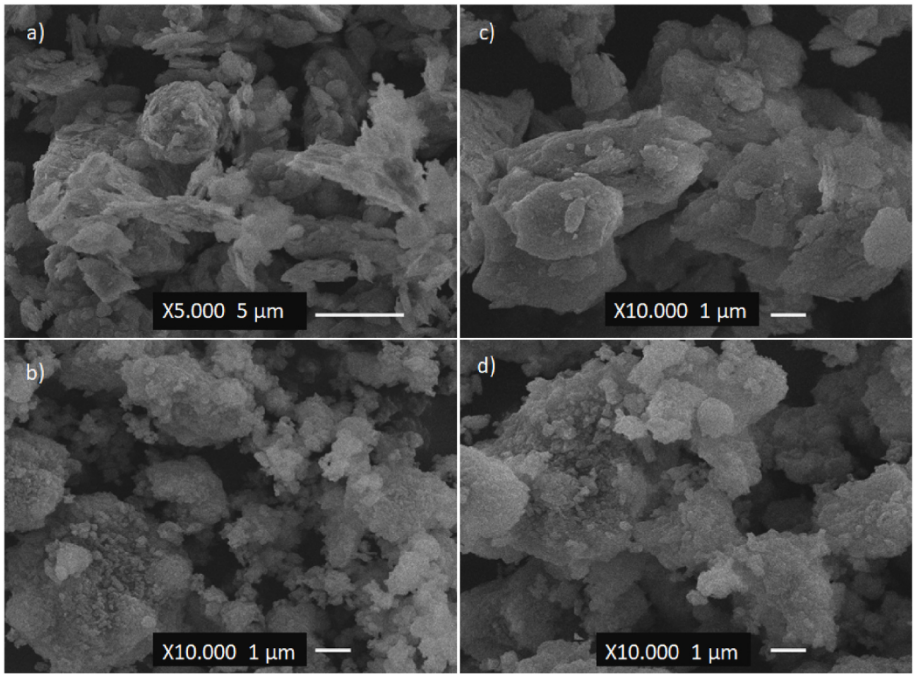

Fig. 3. SEM images of a) $Clay_M$ (x5.000), b) $LaFeClay_M$, c) ZSM5 zeolite and d) LaFeZSM5 with the same resolution (x10.000).

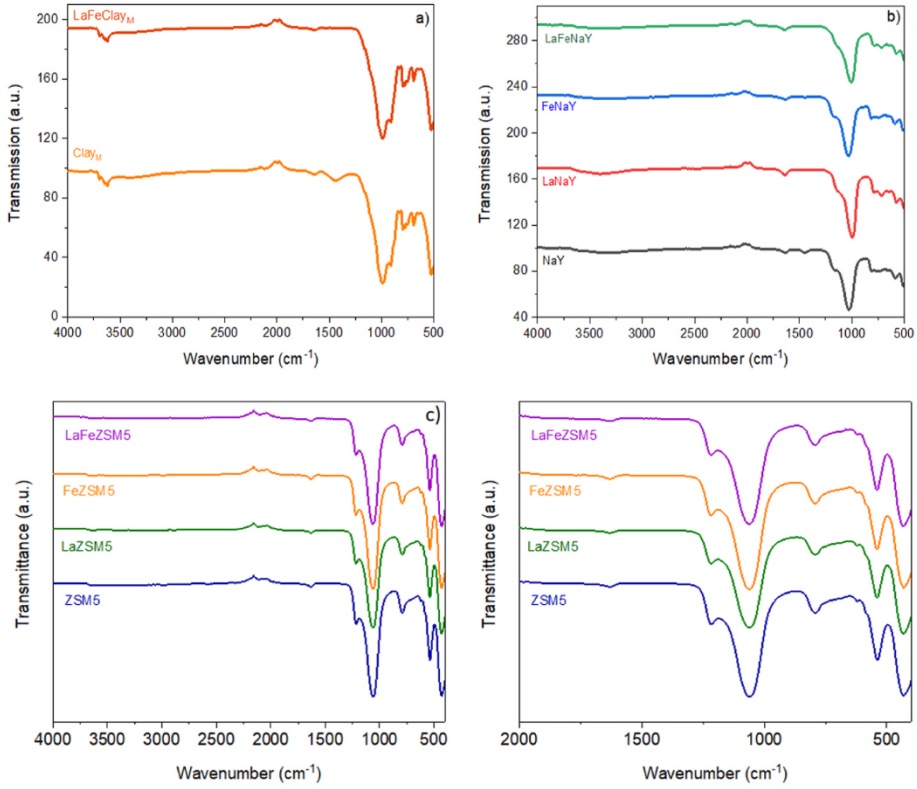

Fig. 4. FTIR spectra of a) $Clay_M$ and $LaFeClay_M$; b) NaY, LaNaY, FeNaY and LaFeNaY and c) ZSM5, LaZSM5, FeZSM5 and LaFeZSM5.

(Al, Al, O)–OH, (Al, Fe, O)–OH and (Al, Mg, O)–OH, which are due to the OH groups on the edge of the clay platelets, and to the bending vibrations of Si–O–Al, respectively [42,43]. After the metal ion-exchanged, the bimetallic catalyst displays the same absorption bands at identical position (Fig. 4a), which confirm that the amount of lanthanum does not affect the clay structure, in agreement of SEM analysis.

For the zeolite samples, the bands in the range 3700–3000 cm^{-1} are ascribed to surface hydroxyl groups, while the characteristic $\delta(H_2O)$ vibration mode of absorbed water corresponds to the band at 1640 cm^{-1}. Furthermore, the bands ascribable to the lattice vibrations associated with the structures are identified in the spectral region between 1300 and 450 cm^{-1} [42,44]. The monometallic and bimetallic catalysts prepared with NaY (Fig. 4b) and ZSM5 (Fig. 4c) exhibit similar absorption bands as of the pristine supports, suggesting that the metals

ion-exchanged do not affect the zeolite structures. However, the band at 1440 cm^{-1} in both NaY and $Clay_M$ supports disappeared after metal ion-exchanged in the catalysts, which could be ascribed to the presence of metal species in the catalysts structure (Fig. 4a and b).

Noteworthy, the absence of a band at 710-700 cm^{-1} in the FTIR spectrum of LaFeZSM5 (Fig. 4c) is attributed to a migration of the Fe ions from the framework to extra-framework positions [41]. The presence of La and Fe species ion-exchanged on ZSM5, together with the acidity behavior of the zeolite endorse the Fenton-like oxidation for degradation of Tar and Caf pollutants.

From TPR analysis (data not shown), a profile similar to that of the pristine support was detected for the bimetallic $LaFeClay_M$ catalyst, with a broad reduction peak centered at 630 °C, indicating that the presence of La^{3+} does not affect the clay framework. However, the bimetallic catalysts prepared with zeolites do not display any reduction peaks, due to the lower amount of the metal species ion-exchanged and their good dispersion into the zeolite structures. A similar behavior was observed for heterogeneous catalysts prepared with palladium ion-exchanged in NaY zeolite [45].

N_2 adsorption/desorption isotherms acquired at −196 °C for the heterogeneous catalysts are described in Fig. S2, where those of the pristine supports are also reported for comparison. According to the IUPAC classification, both $Clay_M$ and the bimetallic catalyst present a Type IIb isotherm with a hysteresis loop, characteristic of clays with mesoporous nature [46]. Type I isotherms typical for microporous solids are shown by all the zeolite-based catalysts; however, the presence of some mesoporosity, especially in the case of ZSM5 and the derived catalysts, is highlighted by the appearance of hysteresis loops [47]. The resulting textural parameters are summarized in Table 4. It can be observed from the figures that, whatever the support, the addition of La and/or Fe does not modify the shape of the original isotherms.

As expected, both the BET surface area (S_{BET}) and pore volume (V_{total}) of clays are much lower compared to those of zeolites, whose values are almost unaffected after the addition of La. On the other hand, a decrease in such parameters can be observed for the ion-exchanged catalysts in comparison with the pristine support, for both the NaY- and ZSM5-based samples. Noteworthy, in contrast with the ZSM5-based ones, the addition of La and/or Fe leads to an increase in V_{meso}, for the NaY-supported samples, particularly evident for the monometallic ones.

3.2. Pollutants degradation by Fenton-like oxidation with LaFeZSM5

The validation of the optimized experimental conditions was performed in order to verify the values predicted by the mathematical model. For that, ZSM5, LaZSM5, FeZSM5 and LaFeZSM5 were used as heterogeneous catalysts to check their performance in the degradation of the pollutants under the optimized experimental parameters. The influence of H_2O_2 as the oxidant in the presence of pollutants was also evaluated.

Fig. 5 shows the catalytic results for the Fenton-like oxidation for Tar (Fig. 5a) and Caf (Fig. 5b), using 0.8 g/L of catalysts, which are in significant agreement with the theoretical values indicated by the model.

Control tests carried out in the presence of only hydrogen peroxide (H_2O_2 – red curves), the pristine zeolite (ZSM5 – blue curves) or the LaFeZSM5 catalyst (green curves) showed negligible conversions of both Tar and Caf.

When H_2O_2 and the heterogeneous catalysts are simultaneously present, remarkably improved performances are obtained, proving that the reaction follows a typical Fenton-like process. For both Tar and Caf compounds the degradation by Fenton-like oxidation in the presence of the heterogeneous catalysts follows the same trend (LaZSM5 < FeZSM5 < LaFeZSM5). Concerning the monometallic catalysts, higher conversions are shown for FeZSM5 (violet curves) in comparison with LaZSM5 (orange curves), with much more notable differences in the case of Tar. This is not surprising since iron is a crucial metal for Fenton reactions, as already reported in other works [15–17,20,35,36,49,50]. Interestingly, for both pollutants, the catalyst LaZSM5 (orange curves) shows

Table 4
Physicochemical properties of the parent supports and the samples.

Samples	S_{BET} (m^2/g)[a]	V_{total} (cm^3/g)[b]	S_{meso} (m^2/g)[c]	V_{micro} (cm^3/g)[c]	V_{meso} (cm^3/g)[e]
$Clay_M$	23	0.039	23	0	0.039
$LaFeClay_M$	22	0.043	22	0	0.043
NaY	792	0.378	19	0.340	0.038
FeNaY	623	0.344	87	0.222	0.122
LaNaY	536	0.256	88	0.106	0.150
LaFeNaY	586	0.272	83	0.208	0.064
ZSM5	401	0.260	185	0.091	0.169
FeZSM5	347	0.197	141	0.087	0.110
LaZSM5	355	0.203	174	0.076	0.127
LaFeZSM5	347	0.201	127	0.091	0.110

[d]Mesopore volume calculated by the difference V_{total}-$V_{micro.}$ [48].
[a] Surface area calculated from the BET equation.
[b] Total pore volume determined from the amount adsorbed at $P/P_o = 0.95$.
[c] External surface area and micropore volume calculated by the *t*-method.

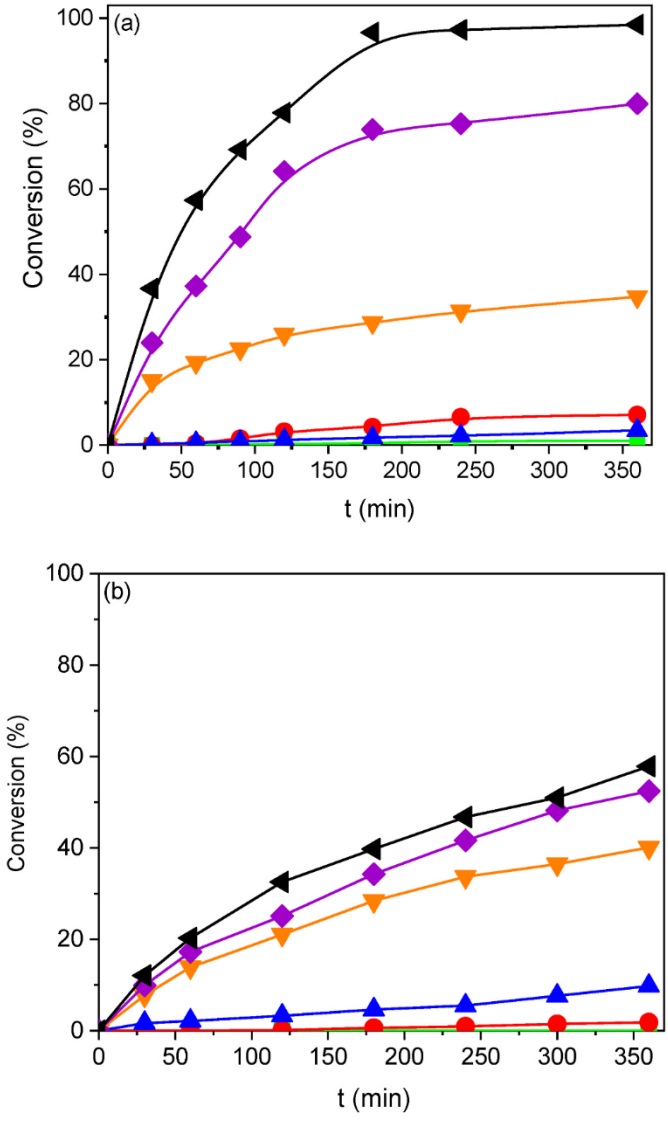

Fig. 5. Conversion of a) Tar and b) Caf versus reaction time over H_2O_2 (red curves), ZSM5 (blue curves), LaFeZSM5 (green curves), LaZSM5 + H_2O_2 (orange curves), FeZSM5 + H_2O_2 (violet curves) and LaFeZSM5 + H_2O_2 (black curves). (For interpretation of the references to color in this figure legend, the reader is referred to the Web version of this article).

comparable conversions with 34.7% and 40.1% for Tar and Caf, respectively. By converse, remarkable differences in the degradation of the two pollutants are observed in the presence of the bimetallic catalyst. Indeed, 96.6% of Tar was degraded after 180 min of reaction, with a mineralization efficiency of 45.5%, whereas only 58% of Caf was converted after 300 min, with a comparable degree of mineralization, 47.0%. The highest conversion values are obtained with the LaFeZSM5 catalyst, indicating that the synergistic effect of the two metal ions together with the acid properties of ZSM5 allow the optimal combination for achieving the best catalytic performance, especially in the case of Tar.

The stability and reusability of the best catalyst in the Fenton-like degradation of Tar and Caf were studied during four cycles and at the end of each cycle TOC was quantified (Fig. 6). Fig. 6a depicts that the bimetallic catalyst is very stable in the case of Tar, with conversions above 96% and important mineralization efficiencies of 45.5% preserved during the four cycles. On the other hand, LaFeZSM5 loses its activity in the degradation of Caf, whose conversion decreases significantly after each reaction cycle (Fig. 6b). However, the X_{caf}/TOC ratio remains almost constant during the reusability test, varying between 1.10 (1° cycle) and 1.25 (4° cycle), indicating that the catalyst maintains its mineralization capacity despite the worsening of the degradation performance.

FTIR and SEM/EDX analyses of the catalyst were performed after the fourth cycle of the reusability tests in the degradation of both Tar and Caf. FTIR spectra of LaFeZSM5 before and after the last recycling tests are very similar to that of the pristine zeolite, demonstrating the stability of the catalyst during the Fenton-like degradation (Fig. 6c) and indicating that the structure of the catalyst is preserved during such reaction.

After Tar degradation, EDX analysis confirms the absence of leaching phenomena for both La and Fe metal ions. In the EDX spectrum of LaFeZSM5 after Caf degradation (Fig. 6d), only iron is detected, probably La is leaching. The loss of the La ions could explain the decrease in the Caf oxidation activity of LaFeZSM5, while it does not seem to affect the mineralization efficiency, as suggested by the constant value of the X_{caf}/TOC ratio.

At the end of the Tar degradation, no leaching of La or Fe was detected (within the experimental error), revealing that the LaFeZSM5 are stable. However, after Caf degration only Fe was detected in agreement with EDX analysis.

Electro Fenton-like oxidation was carried out in the degradation of caffeine without using hydrogen peroxide at room temperature. The cyclic voltammetry (CV) recorded at a scan rate of 100 mV s^{-1} in the absence of Caf (black lines) and in the presence of Caf (red lines) is displayed in Fig. 7a and b. In the absence of Caf, two redox processes were identified: one recorded at −0.30 *vs.* SCE and another at 0.56 V *vs.* SCE. These values are related to the different metal species, the first one probably attributed to the La(0)/La(III) couple while the second one is attributed to Fe(II)/Fe(III) couple [24,41,51].

The presence of La species in the La-mordonite electrode was also studied by Ismail et al., and the authors mentioned that enhances the oxidation process and a reproducible anodic and cathodic peak ascribed to $Fe(CN)_6^{3-}/Fe(CN)_6^{4-}$ redox couple at the surface of the electrode (0.17/0.30 V vs. SCE) was observed, proving that La species are available for the redox processes [51].

The oxidation of Caf (100 ppm) starts at 0.8 V *vs.* SCE corresponding to potential values higher to that observed for Fe(III)/Fe(II) redox couple, suggesting that the presence of both metal species, specially Fe (III) species, on the electrode surface improves the oxidation of the compound. The cyclic voltammetry (CV) at the end of the electrolysis (during 90 min) of Caf over LaFeZSM5 modified electrode in Na_2SO_4 (0.1 M) recorded with a scan rate is 100 mV s^{-1}, suggests that the modified electrode keeps its redox process, showing the stability of the

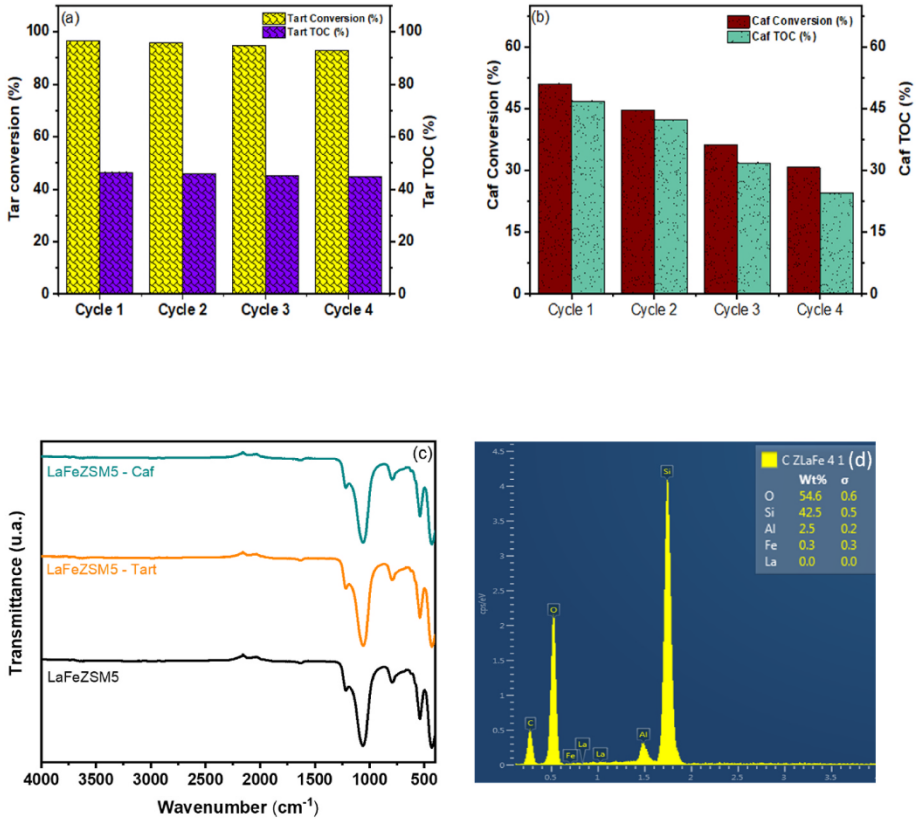

Fig. 6. Conversion and TOC percentages during the consecutive degradation cycles for Tar (a) and Caf (b) over LaFeZSM5; FTIR (c) and (d) EDX spectra at the end of the last cycle of Caf.

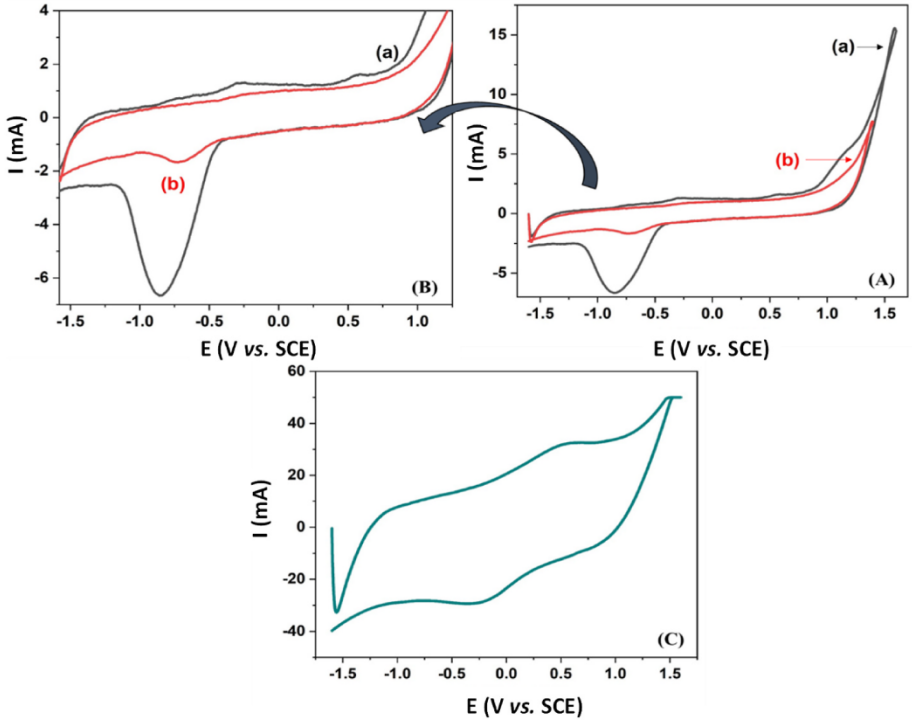

Fig. 7. Cyclic voltammograms (A, B) of LaFeZSM5 modified electrode recorded at 100 mV/s in the absence of Caf (a) and in the presence of Caf (100 ppm, b); (C) at the end of the electrolysis of Caf (100 ppm) at the LaFeZSM5 modified electrode in Na_2SO_4 (0.1 M).

electrode (Fig. 7c).

The electrolysis of Caf (100 ppm) on the LaFeZSM5 modified electrode at 2.0 V *vs.* SCE at room temperature, shows that the degradation of the pristine compound after 90 min achieves 62.4% of conversion with 20.8% of mineralization (Fig. 8). Our results show that the electro Fenton-like oxidation increases the degradation of Caf compared with the Fenton-like reaction (51%, 30 ppm).

Identification of the products during the electrolysis was carried out by HPLC-ESI/MS analysis, since the initial concentration of Caf was 100 ppm, for better resolution. Such analysis allowed several compounds deriving from the degradation product of Caf and to suggest the formation of the intermediate products up to mineralization. The formation

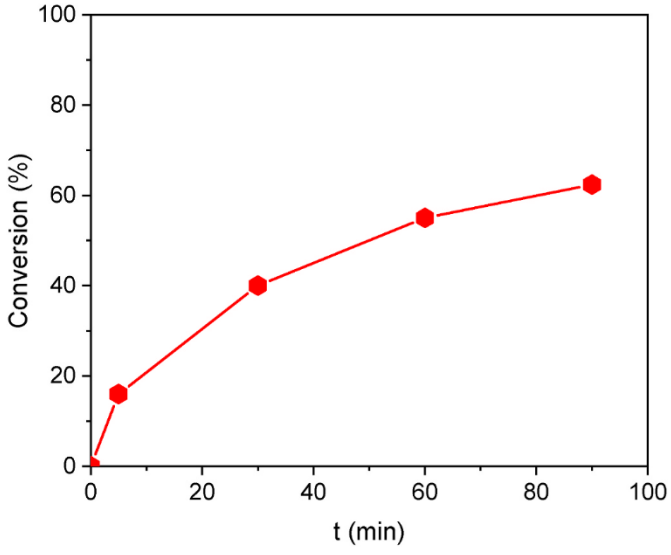

Fig. 8. The evolution of the conversion of Caf in the LaFeZSM5 modified electrode.

of the intermediate compounds during Caf degradation confirms that the oxidation was promoted by the electro-generation of the oxygenated radical species [42]. In both Fenton-like processes, the oxidant agents are the $OH^{\bullet}$ radicals, which are responsible for the formation of the compounds identified up to the mineralization. 8 intermediates were identified in the products of the electrolysis, in which the C1, C2, and C3 compounds are aromatic, while the C4 to C7 compounds are aliphatic. The molecular weight and the structural formula of the identified products are presented in Table S4, and their ESI/MS spectra are displayed in Fig. S4.

Some of these compounds were described in the literature concerning the degradation pathways pathways of caffeine over Co-MCM41 [52]. The identified compounds and the different pathways are due to the presence of $OH^{\bullet}$ and $SO_4^{\bullet-}$ radicals, which are responsible for the attack to the N=C double bond of the purine structure of the Caf molecule [14,52].

A catalytic degradation pathway of Caf at LaFeZSM5 modified electrode could be proposed taking into account the compounds C1, C2, C3, C4, the low molecular weight organic acids, and the mineralization (Fig. 9).

Two pathways are proposed. Pathway 1 is comparable to one of the pathways described in [52]. The compound C1 is similar to the hydroxylated form of the 1,3,7-trimethyluric acid, which contains two additional oxygen atoms over the Caf molecule [52]. In pathway 2, a new compound is proposed, C2, coming from the loss of a methyl group in the Caf molecule. Both pathways lead to C3, known as a biological metabolite of Caf [52], which is produced from C1 and C2. C3 is obtained from pathway 1 by the loss of OH and protonation of N atoms, CO and methyl group. The same product is obtained from the pathway 2 by the attack of the $OH^{\bullet}$ radicals to the C=C bond. The generation of carbonyl groups leads to the opening of the six-member ring C3 [52] with the formation of C4 that, following the total opening of the ring, evolves towards the low molecular weight organic acids (Table S4). These acids, identified as tartronic acid, oxamic acid, oxalic acid and propionic acid by HPLC analysis, continue to suffer attacks from the radicals up to the mineralization.

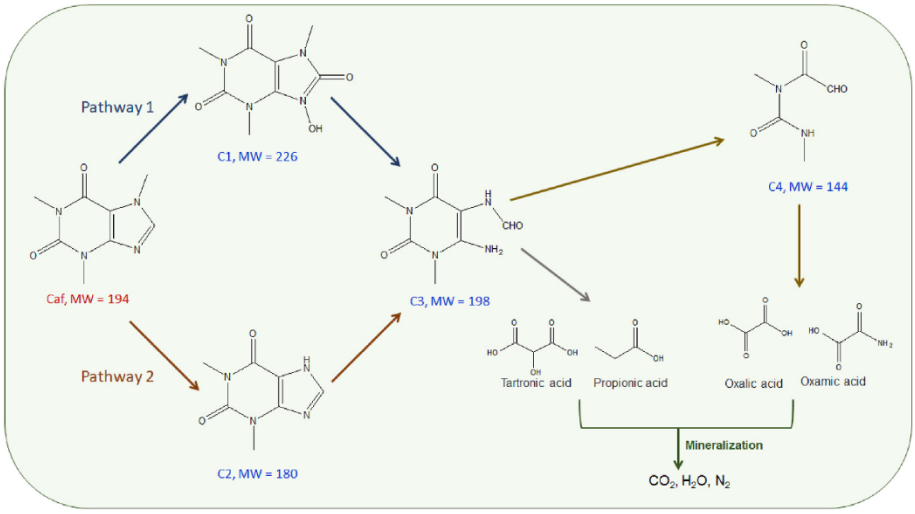

Fig. 9. Proposed pathways for Fenton-like degradation of Caf molecule by LaFeZSM5.

4. Conclusions

Three heterogeneous catalysts based in lanthanum(III) and iron(III) ions ion-exchanged on two zeolite structures and a natural clay from Morocco were evaluated in Fenton-like processes in order to degrade two pollutants in water, tartrazine (Tar) and caffeine (Caf). The effect of different experimental parameters on both pollutants degradation was determined by Box-Behenken design and high catalytic efficiency was obtained with 96.6% and 51.0% degradation of Tar and Caf, respectively, in the presence of LaFeZSM5. For the best catalyst, higher mineralization rates were obtained in Fenton-like oxidation with 45.5% for Tar and 47.0% for Caf. The degradation of Caf was improved by electro Fenton-like oxidation with 62.4% of Caf conversion after 90 min over the modified LaFeZSM5 electrode. The higher conversion obtained in this work by Fenton-like processes for the degradation of pollutants in water highlighted the importance of the validation of the optimized experimental conditions by mathematical models.

CRediT authorship contribution statement

Ouissal Assila: Writing – original draft, Software, Formal analysis, Data curation. **Óscar Barros:** Writing – original draft, Investigation, Formal analysis, Data curation. **António M.F. Fonseca:** Writing – review & editing, Writing – original draft, Investigation, Funding acquisition. **Pier Parpot:** Writing – review & editing, Writing – original draft, Visualization, Supervision, Investigation. **Olívia S.G.P. Soares:** Writing – review & editing, Writing – original draft, Validation, Investigation. **Manuel F.R. Pereira:** Writing – review & editing, Writing – original draft, Visualization, Validation. **Farid Zerrouq:** Writing – review & editing, Validation. **Abdelhak Kherbeche:** Writing – review & editing, Visualization, Validation. **Elizabetta Rombi:** Writing – review & editing, Writing – original draft, Visualization, Validation, Resources, Investigation. **Teresa Tavares:** Writing – review & editing, Writing – original draft, Validation, Supervision, Resources, Project administration, Funding acquisition. **Isabel C. Neves:** Writing – review & editing, Writing – original draft, Validation, Supervision, Project administration, Funding acquisition, Conceptualization.

Declaration of competing interest

The authors declare that they have no known competing financial interests or personal relationships that could have appeared to influence the work reported in this paper.

Data availability

Data will be made available on request.

Acknowledgements

O.A. thanks to ERASMUS + Program for the mobility Ph.D. grant and O.B. thanks to Fundação para Ciência e Tecnologia, Portugal (FCT) for his Ph.D. grant (SFRH/BD/140362/2018).This research work has been funded by national funds funded through FCT/MCTES (PIDDAC) over the projects: LA/P/0045/2020 (ALiCE), UIDB/50020/2020 and UIDP/50020/2020 (LSRE-LCM), UIDB/04469/2020 (CEB) and by LA/P/0029/2020 (LABBELS), Centre of Chemistry (UID/QUI/0686/2020) and project BioTecNorte (operation NORTE-01-0145-FEDER-000004), supported by the Northern Portugal Regional Operational Programme (NORTE 2020), under the Portugal 2020 Partnership Agreement, through the European Regional Development Fund (ERDF).

Appendix A. Supplementary data

Supplementary data to this article can be found online at https://doi.org/10.1016/j.micromeso.2022.112422.

References

[1] B. Zheng, J. Fan, B. Chen, X. Qin, J. Wang, F. Wang, R. Deng, X. Liu, Rare-earth doping in nanostructured inorganic materials, Chem. Rev. 122 (2022) 5519–5603, https://doi.org/10.1021/acs.chemrev.1c00644.
[2] Y. Xin, H. Liu, Study on mechanism of photocatalytic performance of La-doped TiO2/Ti photoelectrodes by theoretical and experimental methods, J. Solid State Chem. 184 (2011) 3240–3246, https://doi.org/10.1016/j.jssc.2011.10.017.
[3] L. Wang, Y. Ma, Y. Wang, S. Liu, Y. Deng, Efficient synthesis of glycerol carbonate from glycerol and urea with lanthanum oxide as a solid base catalyst, Catal. Commun. 12 (2011) 1458–1462, https://doi.org/10.1016/j.catcom.2011.05.027.
[4] Y. Wei, S. Zhang, S. Yin, C. Zhao, S. Luo, C.T. Au, Solid superbase derived from lanthanum-magnesium composite oxide and its catalytic performance in the knoevenagel condensation under solvent-free condition, Catal. Commun. 12 (2011) 1333–1338, https://doi.org/10.1016/j.catcom.2011.05.010.
[5] X. Zheng, H. Lin, J. Zheng, X. Duan, Y. Yuan, Lanthanum oxide-modified Cu/SiO2 as a high-performance catalyst for chemoselective hydrogenation of dimethyl oxalate to ethylene glycol, ACS Catal. 3 (2013) 2738–2749, https://doi.org/10.1021/cs400574v.
[6] L. Li, X. Wang, Y. Zhang, Enhanced visible light-responsive photocatalytic activity of LnFeO 3 (ln = La, Sm) nanoparticles by synergistic catalysis, Mater. Res. Bull. 50 (2014) 18–22, https://doi.org/10.1016/j.materresbull.2013.10.027.
[7] J. Liu, Z. Zhao, C. ming Xu, A. jun Duan, Simultaneous removal of NOx and diesel soot over nanometer ln-Na-Cu-O perovskite-like complex oxide catalysts, Appl. Catal. B Environ. 78 (2008) 61–72, https://doi.org/10.1016/j.apcatb.2007.09.001.
[8] P. Chen, B. Lei, X. Dong, H. Wang, J. Sheng, W. Cui, J. Li, Y. Sun, Z. Wang, F. Dong, Rare-earth single-atom La-N charge-transfer bridge on carbon nitride for highly

efficient and selective photocatalytic CO2 reduction, ACS Nano 14 (2020) 15841–15852, https://doi.org/10.1021/acsnano.0c07083.
[9] E.F. Sousa-Aguiar, F.E. Trigueiro, F.M.Z. Zotin, The role of rare earth elements in zeolites and cracking catalysts, Catal. Today 218–219 (2013) 115–122, https://doi.org/10.1016/j.cattod.2013.06.021.
[10] T.V. Malleswara Rao, X. Dupain, M. Makkee, Fluid catalytic cracking: processing opportunities for fischer-tropsch waxes and vegetable oils to produce transportation fuels and light olefins, Microporous Mesoporous Mater. 164 (2012) 148–163, https://doi.org/10.1016/j.micromeso.2012.07.016.
[11] O.D. Mante, F.A. Agblevor, S.T. Oyama, R. McClung, The effect of hydrothermal treatment of FCC catalysts and ZSM-5 additives in catalytic conversion of biomass, Appl. Catal. Gen. 445–446 (2012) 312–320, https://doi.org/10.1016/j.apcata.2012.08.039.
[12] L. Chen, D. Zhang, Y. Chen, F. Liu, J. Zhang, M. Fu, J. Wu, D. Ye, Porous stainless-steel fibers supported CuCeFeOx/zeolite catalysts for the enhanced CO oxidation: experimental and kinetic studies, Chemosphere 291 (2022), 132778, https://doi.org/10.1016/j.chemosphere.2021.132778.
[13] H. Liu, M. Cheng, Y. Liu, J. Wang, G. Zhang, L. Li, L. Du, G. Wang, S. Yang, X. Wang, Single atoms meet metal–organic frameworks: collaborative efforts for efficient photocatalysis, Energy Environ. Sci. 15 (2022) 3722, https://doi.org/10.1039/d2ee01037b.
[14] Q. Shi, S. Deng, Y. Zheng, Y. Du, L. Li, S. Yang, G. Zhang, L. Du, G. Wang, M. Cheng, Y. Liu, The application of transition metal-modified biochar in sulfate radical based advanced oxidation processes, Environ. Res. 212 (2022), 113340, https://doi.org/10.1016/j.envres.2022.113340.
[15] W. Fu, J. Yi, M. Cheng, Y. Liu, G. Zhang, L. Li, L. Du, B. Li, G. Wang, X. Yang, When bimetallic oxides and their complexes meet Fenton-like process, J. Hazard Mater. 424 (2022), 127419, https://doi.org/10.1016/j.jhazmat.2021.127419.
[16] Y. Liu, Y. Zhao, J. Wang, Fenton/Fenton-like processes with in-situ production of hydrogen peroxide/hydroxyl radical for degradation of emerging contaminants: advances and prospects, J. Hazard Mater. 404 (2021), 124191, https://doi.org/10.1016/j.jhazmat.2020.124191.
[17] J. Wang, J. Tang, Fe-based Fenton-like catalysts for water treatment: preparation, characterization and modification, Chemosphere 276 (2021), 130177, https://doi.org/10.1016/j.chemosphere.2021.130177.
[18] A.R. Ribeiro, O.C. Nunes, M.F.R. Pereira, A.M.T. Silva, An overview on the advanced oxidation processes applied for the treatment of water pollutants defined in the recently launched directive 2013/39/EU, Environ. Int. 75 (2015) 33–51, https://doi.org/10.1016/j.envint.2014.10.027.
[19] H. Fida, G. Zhang, S. Guo, A. Naeem, Heterogeneous Fenton degradation of organic dyes in batch and fixed bed using La-Fe montmorillonite as catalyst, J. Colloid Interface Sci. 490 (2017) 859–868, https://doi.org/10.1016/j.jcis.2016.11.085.
[20] B.L.C. Santos, P. Parpot, O.S.G.P. Soares, M.F.R. Pereira, E. Rombi, A.M. Fonseca, I. C. Neves, Fenton-type bimetallic catalysts for degradation of dyes in aqueous solutions, Catalysts 11 (2021) 32, https://doi.org/10.3390/catal11010032.
[21] O. Assila, M. Zouheir, K. Tanji, R. Haounati, F. Zerrouq, A. Kherbeche, Copper nickel Co-impregnation of Moroccan yellow clay as promising catalysts for the catalytic wet peroxide oxidation of caffeine, Heliyon 7 (2021), e06069, https://doi.org/10.1016/j.heliyon.2021.e06069.
[22] A.G. Trovó, T.F.S. Silva, O. Gomes, A.E.H. Machado, W.B. Neto, P.S. Muller, D. Daniel, Degradation of caffeine by photo-fenton process: optimization of treatment conditions using experimental design, Chemosphere 90 (2013) 170–175, https://doi.org/10.1016/j.chemosphere.2012.06.022.
[23] L. Elleuch, M. Messaoud, K. Djebali, M. Attafi, Y. Cherni, M. Kasmi, A. Elaoud, I. Trabelsi, A. Chatti, A new insight into highly contaminated landfill leachate treatment using kefir grains pre-treatment combined with Ag-doped TiO2 photocatalytic process, J. Hazard Mater. 382 (2020), 121119, https://doi.org/10.1016/j.jhazmat.2019.121119.
[24] M. Ferreira, N.E. Sahin, A.M. Fonseca, P. Parpot, I.C. Neves, Oxidation of pollutants via an electro-fenton-like process in aqueous media using iron-zeolite modified electrodes, New J. Chem. 45 (2021) 12750–12757, https://doi.org/10.1039/d1nj01077h.
[25] Ó. Barros, L. Costa, F. Costa, A. Lago, V. Rocha, Z. Vipotnik, B. Silva, T. Tavares, Recovery of rare earth elements from wastewater towards a circular economy, Molecules 24 (2019), https://doi.org/10.3390/molecules24061005.
[26] O. Assila, Y. Miyah, L. Nahali, A. EL Badraoui, V. Nenov, B. EL Khazzan, F. Zerrouq, A. Kherbeche, Copper-impregnated on natural material as promising catalysts for the wet hydrogen peroxide catalytic oxidation of methyl green, Moroc. J. Chem. 9 (2021), 084–101.
[27] O. Assila, K. Tanji, M. Zouheir, A. Arrahli, L. Nahali, F. Zerrouq, A. Kherbeche, Adsorption studies on the removal of textile effluent over two natural eco-friendly adsorbents, J. Chem. (2020) 13, https://doi.org/10.1155/2020/6457825, 2020.
[28] M. Ferreira, I. Kuzniarska-Biernacka, A.M. Fonseca, I.C. Neves, O.S.G.P. Soares, M. F.R. Pereira, J.L. Figueiredo, P. Parpot, Study of the electroreactivity of amoxicillin on carbon nanotubes supported metal electrodes, ChemCatChem 10 (2018) 4914–4923, https://doi.org/10.1002/cctc.201801193.
[29] A.M. Fonseca, S. Goncalves, P. Parpot, I.C. Neves, Host–guest Chemistry of the (N, N'diarylacetamidine)Rhodium(III) complex in zeolite Y, Phys. Chem. Chem. Phys. 11 (2009) 6308–6314, https://doi.org/10.1039/b816698f.
[30] S. Ahmad Bhawani, S.S. Fong, M.N. Mohamad Ibrahim, Spectrophotometric analysis of caffeine, Int. J. Anal. Chem. (2015) 7, https://doi.org/10.1155/2015/170239, 2015.
[31] A. Ziylan-Yavas, N.H. Ince, E. Ozon, E. Arslan, V. Aviyente, B. Savun-Hekimoğlu, A. Erdincler, Oxidative decomposition and mineralization of caffeine by advanced oxidation processes: the effect of hybridization, Ultrason. Sonochem. 76 (2021), 105635, https://doi.org/10.1016/j.ultsonch.2021.105635.
[32] S. Perveen, R. Nadeem, M. Iqbal, S. Bibi, R. Gill, R. Saeed, S. Noreen, K. Akhtar, T. Mehmood Ansari, N. Alfryyan, Graphene oxide and Fe3O4 composite synthesis, characterization and adsorption efficiency evaluation for NO_3^- and PO_4^{3-} ions in aqueous medium, J. Mol. Liq. 339 (2021), 116746, https://doi.org/10.1016/j.molliq.2021.116746.
[33] M.E.M. Ali, H. Abdelsalam, N.S. Ammar, H.S. Ibrahim, Response surface methodology for optimization of the adsorption capability of ball-milled pomegranate peel for different pollutants, J. Mol. Liq. 250 (2018) 433–445, https://doi.org/10.1016/j.molliq.2017.12.025.
[34] A. Tabasum, M. Zahid, H.N. Bhatti, M. Asghar, Fe3O4-GO composite as efficient heterogeneous photo-fenton's catalyst to degrade pesticides, Mater. Res. Express (2018) 11–14, https://doi.org/10.1088/2053-1591/aae6ab.
[35] M.L. Rache, A.R. García, H.R. Zea, A.M.T. Silva, L.M. Madeira, J.H. Ramírez, Azo-dye orange II degradation by the heterogeneous fenton-like process using a zeolite Y-Fe catalyst-kinetics with a model based on the fermi's equation, Appl. Catal. B Environ. 146 (2014) 192–200, https://doi.org/10.1016/j.apcatb.2013.04.028.
[36] J. Feng, X. Hu, P.L. Yue, Effect of initial solution PH on the degradation of orange II using clay-based Fe nanocomposites as heterogeneous photo-fenton catalyst, Water Res. 40 (2006) 641–646, https://doi.org/10.1016/j.watres.2005.12.021.
[37] C.R. Reddy, Y.S. Bhat, G. Nagendrappa, B.S. Jai Prakash, Brønsted and Lewis acidity of modified montmorillonite clay catalysts determined by FT-IR spectroscopy, Catal. Today 141 (2009) 157–160, https://doi.org/10.1016/j.cattod.2008.04.004.
[38] H.V. Lee, J.C. Juan, Y.H. Taufiq-Yap, Preparation and application of binary acid-base CaO-La2O3 catalyst for biodiesel production, Renew. Energy 74 (2015) 124–132, https://doi.org/10.1016/j.renene.2014.07.017.
[39] P. Peixoto, J.F. Guedes, E. Rombi, A.M. Fonseca, C.A. Aguiar, I.C. Neves, Metal ion-zeolite materials against resistant bacteria, MRSA, Ind. Eng. Chem. Res. 60 (2021) 12883–12892, https://doi.org/10.1021/acs.iecr.1c01736.
[40] C.M.A.S. Freitas, O.S.G.P. Soares, J.J.M. Órfão, A.M. Fonseca, M.F.R. Pereira, I. C. Neves, Highly efficient reduction of bromate to bromide over mono and bimetallic ZSM5 catalysts, Green Chem. 17 (2015) 4247–4254, https://doi.org/10.1039/c5gc00777a.
[41] Z. Bencheqroun, N.E. Sahin, O.S.G.P. Soares, M.F.R. Pereira, H. Zaitan, M. Nawdali, E. Rombi, A.M. Fonseca, P. Parpot, I.C. Neves, Fe (III) -exchanged zeolites as efficient electrocatalysts for fenton-like oxidation of dyes in aqueous phase, J. Environ. Chem. Eng. 10 (2022), 107891, https://doi.org/10.1016/j.jece.2022.107891.
[42] J.C. Villalba, V.R.L. Constantino, F.J. Anaissi, Iron oxyhydroxide nanostructured in montmorillonite clays: preparation and characterization, J. Colloid Interface Sci. 349 (2010) 49–55, https://doi.org/10.1016/j.jcis.2010.04.057.
[43] X. Xu, Y. Ding, Z. Qian, F. Wang, B. Wen, H. Zhou, S. Zhang, M. Yang, Degradation of poly(ethylene terephthalate)/clay nanocomposites during melt extrusion: effect of clay catalysis and chain extension, Polym. Degrad. Stabil. 94 (2009) 113–123, https://doi.org/10.1016/j.polymdegradstab.2008.09.009.
[44] F. Costa, C.J.R. Silva, M.M.M. Raposo, A.M. Fonseca, I.C. Neves, A.P. Carvalho, J. Pires, Synthesis and immobilization of molybdenum complexes in a pillared layered clay, Microporous Mesoporous Mater. 72 (2004) 111–118, https://doi.org/10.1016/j.micromeso.2004.04.003.
[45] O.S.G.P. Soares, L. Marques, C.M.A.S. Freitas, A.M. Fonseca, P. Parpot, J.J. M. Órfão, M.F.R. Pereira, I.C. Neves, Mono and bimetallic NaY catalysts with high performance in nitrate reduction in water, Chem. Eng. J. 281 (2015) 411–417, https://doi.org/10.1016/j.cej.2015.06.093.
[46] M. Saidian, L.J. Godinez, M. Prasad, Effect of clay and organic matter on nitrogen adsorption specific surface area and cation exchange capacity in shales (mudrocks), J. Nat. Gas Sci. Eng. 33 (2016) 1095–1106, https://doi.org/10.1016/j.jngse.2016.05.064.
[47] C. Ferreira, A. Araujo, V. Calvino-Casilda, M.G. Cutrufello, E. Rombi, A.M. Fonseca, M.A. Bañares, I.C.Y. Neves, Zeolite-supported niobium pentoxide catalysts for the glycerol acetalization reaction, Microporous Mesoporous Mater. 271 (2018) 243–251, https://doi.org/10.1016/j.micromeso.2018.06.010.
[48] N. Vilaça, R. Amorim, A.F. Machado, P. Parpot, M.F.R. Pereira, M. Sardo, J. Rocha, A.M. Fonseca, I.C. Neves, F. Baltazar, Potentiation of 5-fluorouracil encapsulated in zeolites as drug delivery systems for in vitro models of colorectal carcinoma, Colloids Surf. B Biointerfaces 112 (2013) 237–244, https://doi.org/10.1016/j.colsurfb.2013.07.042.
[49] A. Babuponnusami, K. Muthukumar, A review on Fenton and improvements to the Fenton process for wastewater treatment, J. Environ. Chem. Eng. 2 (2014) 557–572, https://doi.org/10.1016/j.jece.2013.10.011.
[50] K.A. Sashkina, E.V. Parkhomchuk, N.A. Rudina, V.N. Parmon, The role of zeolite Fe-ZSM-5 porous structure for heterogeneous Fenton catalyst activity and stability, Microporous Mesoporous Mater. 189 (2014) 181–188, https://doi.org/10.1016/j.micromeso.2013.11.033.
[51] A. Ismail, A. Kawde, O. Muraza, M.A. Sanhoob, A.R. Al-Betar, Lanthanum-impregnated zeolite modified carbon paste electrode for determination of cadmium (II), Microporous Mesoporous Mater. 225 (2016) 164–173, https://doi.org/10.1016/j.micromeso.2015.12.023.
[52] F. Qi, W. Chu, B. Xu, Catalytic degradation of caffeine in aqueous solutions by cobalt-MCM41 activation of peroxymonosulfate, Appl. Catal. B Environ. 134–135 (2013) 324–332, https://doi.org/10.1016/j.apcatb.2013.01.038.